HELDA
HELSINGIN YLIOPISTO
HELSINGFORS UNIVERSITET
UNIVERSITY OF HELSINKI

UNIVERSITY OF HELSINKI

https://helda.helsinki.fi

A combined experimental and theoretical study of small and large vacancy clusters in tungsten

Yang, Qigui

2022-12-01

Yang , Q , Hu , Z , Makkonen , I , Desgardin , P , Egger , W , Barthe , M-F & Olsson , P 2022 , ' A combined experimental and theoretical study of small and large vacancy clusters in tungsten ' , Journal of Nuclear Materials , vol. 571 , 154019 . https://doi.org/10.1016/j.jnucmat.2022.154019

http://hdl.handle.net/10138/351077
https://doi.org/10.1016/j.jnucmat.2022.154019

cc_by
publishedVersion

Downloaded from Helda, University of Helsinki institutional repository.

This is an electronic reprint of the original article.

This reprint may differ from the original in pagination and typographic detail.

Please cite the original version.

Journal of Nuclear Materials 571 (2022) 154019

Contents lists available at ScienceDirect

Journal of Nuclear Materials

journal homepage: www.elsevier.com/locate/jnucmat

A combined experimental and theoretical study of small and large vacancy clusters in tungsten

Qigui Yang[a,1], Zhiwei Hu[b,1], Ilja Makkonen[c], Pierre Desgardin[b], Werner Egger[d], Marie-France Barthe[b,*], Pär Olsson[a,*]

[a] KTH Royal Institute of Technology, Nuclear Engineering, Roslagstullsbacken 21, 114 21 Stockholm, Sweden
[b] CEMHTI, CNRS, UPR3079, University of Orléans, F-45071 Orléans, France
[c] Department of Physics, University of Helsinki, P.O. Box 43, FI-00014 Helsinki, Finland
[d] Institut für Angewandte Physik und Messtechnik, Universität der Bundeswehr München, D-85579 Neubiberg, Germany

ARTICLE INFO

Article history:
Received 31 May 2022
Revised 31 August 2022
Accepted 3 September 2022
Available online 5 September 2022

Keywords:
Positron annihilation spectroscopy
First-principles calculations
Tungsten
Vacancy clusters
Two-component density functional theory

ABSTRACT

Tungsten is considered to be used in the future fusion reactors as plasma-facing material. In such extreme environments, defects are induced in materials that modify their macroscopic properties such as the mechanical ones. It is of paramount importance to be able to determine concentration and size of the vacancy defects, from the mono vacancy to the large cavities, to validate the models developed to predict the evolution of the microstructure of irradiated materials. Positrons are very useful non-destructive probes that can characterize vacancy-type defects in materials. We present a combined experimental and theoretical study on detecting and estimating the sizes of vacancy clusters that are invisible with electron microscopy in tungsten, using positron annihilation spectroscopy. We here model the positron annihilation in the tungsten lattice and in vacancy-type defects using state-of-the-art first principles methodology. The Doppler broadening spectra and positron lifetimes in tungsten are calculated with two-component density functional theory with local density approximation and weighted density approximation. Our calculations are in excellent agreement with our experimental results. We show that the sizes of vacancy clusters in tungsten can be well estimated by combining both positron lifetimes and Doppler broadening spectra. We also determine the limit of validity of the canonical calculation method, which here is shown to fail when the vacancy clusters grow beyond their nucleation stage. This work is a first step needed to better interpret the measured positron annihilation characteristics (Doppler and lifetime) in tungsten and then extract quantitative data on small vacancy defects required to improve the understanding of early-stage vacancy defect evolution in tungsten. The method used in this paper could be used to study other metallic materials.

© 2022 The Authors. Published by Elsevier B.V.
This is an open access article under the CC BY license (http://creativecommons.org/licenses/by/4.0/)

1. Introduction

Tungsten is considered as one of the most promising candidates for plasma-facing materials because of its extraordinary properties, including high melting point, low sputtering yield and excellent radiation resistance [1]. In fusion reactors, tungsten will be exposed to extremely intense neutron irradiation which will cause significant level of radiation damage in terms of isolated Frenkel pairs (vacancies and self-interstitials), self-interstitial and vacancy clusters, as well as defect-solute complexes [1,2]. Vacancy clusters (or voids) in tungsten have been extensively studied both experimentally and theoretically [3–6]. For large vacancy clusters (voids), transmission electron microscopy (TEM) is a powerful technique that can be used to observe and identify their formation and evolution mechanisms. However, the resolution of TEM is limited (usually to ~1 nm), which means that small vacancy clusters cannot be directly observed by TEM. The evolution of small vacancy clusters is also important to have a complete understanding of defect evolution in tungsten and quantitative data (size, concentrations) are of most importance to validate the models which are developed to predict the microstructure evolution under irradiation. Positron annihilation spectroscopy (PAS) is broadly used to study these TEM-invisible defects [7].

Numerous experimental studies with PAS have been performed to study vacancy clusters in tungsten [3,8–10]. In these stud-

* Corresponding authors.
E-mail addresses: marie-france.barthe@cnrs-orleans.fr (M.-F. Barthe), polsson@kth.se (P. Olsson).
[1] These authors contributed equally to this work.

https://doi.org/10.1016/j.jnucmat.2022.154019
0022-3115/© 2022 The Authors. Published by Elsevier B.V. This is an open access article under the CC BY license (http://creativecommons.org/licenses/by/4.0/)

ies, both positron annihilation lifetime spectroscopy (PALS) and Doppler broadening spectroscopy (DBS) were utilized to investigate the vacancy defects induced by irradiation and their evolution. Most of them focused on thick samples damaged by irradiation with high energy electrons, neutrons or light ions for which the PALS measurements can be carried out with fast positrons penetrating deep in matter (a few 100 µm depending on the density). However, irradiation with heavy ions at medium or low energy (from ~100 keV to tens of MeV, depending on their mass) allows to mimic the damage induced by recoils atoms produced by neutron collisions. Such irradiation conditions create damage close to the surface (first 100 nm- a few µm) requiring to use of slow positrons accelerator which are very often coupled to DBS [11] due its easier implementation compare to PALS which requires a pulsed positron beam [12,13]. However, there is a lack of coupling with theoretical calculations and defect modeling. While there are many studies which calculated positron lifetimes of tungsten vacancies [14–16] and Doppler spectra of tungsten lattice [17,18], there is no systematical calculation of the Doppler spectra of tungsten vacancy clusters.

First-principles calculations with two-component density functional theory (TCDFT) are widely used to interpret PAS results, including both local chemical environments and defect sizes [7,19–21]. For perfect lattice and small defects (like single vacancies and vacancy-impurity complexes), it has been shown that this theory in the framework of the local density approximation (LDA) for the electron-positron correlation energy and enhancement factor usually yields reasonably accurate results [7,19,22,23]. Nevertheless, as we will demonstrate in this work, LDA has some problems to correctly calculate the Doppler spectra of larger vacancy clusters since it fails to correctly describe the correlation potential and enhancement factor in vacuum. Therefore, it is challenging to use LDA to study strongly inhomogeneous systems involving non-local correlations, such as surfaces and relatively large vacancy clusters [24]. Although this issue of LDA does not affect the calculation of positron lifetimes of vacancy clusters, the computational Doppler spectra will be problematic, as we will see here in Section 3.2. This requires us to use a more proper model for inhomogeneous systems.

The weighted-density approximation (WDA) is a non-local model which reasonably accurately describes the effects of the screening cloud at the surface when the positron is in the vacuum [25–27]. Recently, Callewaert et al. [24] developed an implementation based on the Rubaszek WDA [27]. In Ref. [24], a thorough test on positron lifetimes of bulk materials with WDA was made, which successfully reproduced experimental positron lifetimes of different materials provided that a materials-specific sum rule involving one free parameter was used. There are also a few recent works [28,29] which show that WDA yields reliable results for surfaces. However, while large vacancy clusters are also inhomogeneous systems, no study by using WDA has yet been reported. Moreover, none of the aforementioned WDA studies calculated Doppler spectra of materials. Positron lifetimes are generally not sufficient to investigate all properties of defects in materials. For a more complete understanding, lifetime calculations should be combined with the Doppler spectra calculations. Therefore, a systematic study of the calculation of Doppler spectra with WDA is highly relevant to estimate the vacancy cluster sizes in tungsten.

In this paper, we present a systematic experimental and theoretical study of vacancy defects in tungsten. For the experimental part, the annihilation characteristics of lattice, single vacancy and the largest detectable vacancy cluster (V_N cluster) are determined by DBS [10]. The detailed experimental results are included in the Appendix. For the theoretical part, we calculate positron lifetimes and Doppler spectra of vacancy clusters in tungsten using both LDA and WDA. The experimental and theoretical results are compared and discussed. We show that the sizes of vacancy clusters can be estimated with theoretical calculations by combining both positron lifetimes and Doppler spectra. This study is expected to improve the understanding of vacancy cluster evolution in tungsten. It is also expected to inspire more theoretical works on inhomogeneous systems with non-local correlations by using TCDFT.

2. Methods

2.1. Computational methods

In this work, the first-principles calculations were performed by using Vienna *Ab initio* Simulation Package (VASP) [30] with the projector augmented wave (PAW) method [31]. The generalized gradient approximation with the Perdew-Burke-Ernzerhof exchange-correlation functional [32] was used for the electron exchange and correlation energy. The $6\times6\times6$ bcc supercells containing 432 lattice sites were used for all calculations. For vacancy cluster structures, instead of using conventional spherical structures, we followed the work of Hou et al. [33] to generate the most stable cluster structures with the minimum formation energy. The plane-wave cutoff energy was set to 230 eV; and a $2\times2\times2$ Γ-centered *k*-point mesh was used for all calculations. We chose the PAW potential which treats the $5p^6 5d^4 6s^2$ electrons as valence states. All supercells containing vacancies were fully relaxed including a self-consistent relaxation taking into account the repulsive forces on the ions due to the localized positron [22]. The positron-induced forces are always calculated with the Boroński-Nieminen LDA [19]. For small vacancy clusters, the LDA relaxation can be expected to be accurate [34]. For large vacancy clusters, the effect of a positron on the local structure can essentially be ignored. The convergence criterion for electronic loop was 10^{-5} eV. The force tolerance for ionic relaxation was 0.01 eV/Å.

After calculating the electron densities, the positron densities and lifetimes were calculated using two different electron-positron correlation potentials, the Boroński-Nieminen LDA [19] and the Rubaszek WDA [27] with Drummond enhancement [35] developed by Callewaert et al. [24]. We here call them LDA and WDA for simplification. In both approximations, the positron was approximated to not affect the average electron density, and the zero-positron-density limit was used [19]. Although the zero-density-limit results in the non-self-consistent treatment of positron densities, it has been shown in Ref. [34] that the non-self-consistent calculation yields very similar results with the fully self-consistent calculations for small vacancy defects. For LDA, the positron lifetime τ is calculated as the inverse of the annihilation rate λ as

$$\lambda = \frac{1}{\tau} = \pi r_e^2 c \int d\mathbf{r} n_e(\mathbf{r}) n_p(\mathbf{r}) \gamma(n_e(\mathbf{r})), \quad (1)$$

where r_e is the classical electron radius, c is the light speed, $n_e(\mathbf{r})$ is the electron density, $n_p(\mathbf{r})$ is the positron density and $\gamma(n_e(\mathbf{r}))$ is the LDA enhancement factor [19]. For WDA, the positron lifetimes are calculated in a modified way, in which the so-called shell partitioning method [24,36,37] is included as

$$\lambda = \frac{1}{\tau} = \pi r_e^2 c \int d\mathbf{r} n_e(\mathbf{r}) n_p(\mathbf{r}) \gamma(\tilde{n}_e(\mathbf{r})), \quad (2)$$

where the enhancement factor is evaluated with the effective electron density $\tilde{n}_e(\mathbf{r})$. According to the shell partitioning method described in Ref. [24], $\tilde{n}_e(\mathbf{r})$ is written as

$$\tilde{n}_e(\mathbf{r}) = n^*_{e,valence}(\mathbf{r}) + n_{e,core}(\mathbf{r}), \quad (3)$$

where $n^*_{e,valence}(\mathbf{r})$ is the effective valence electron density treated by WDA and $n_{e,core}(\mathbf{r})$ is the core electron density treated by LDA [24].

Based on the calculated positron densities, the Doppler spectra were computed with the state-dependent scheme [38] and

PAW method [22]. The momentum density $\rho(\mathbf{p})$ of the annihilating electron-positron pairs are expressed as [7,22]

$$\rho(\mathbf{p}) = \pi r_e^2 c \sum_j \gamma_j \left| \int d\mathbf{r} e^{-i\mathbf{p}\cdot\mathbf{r}} \psi_p(\mathbf{r}) \psi_j(\mathbf{r}) \right|^2, \quad (4)$$

where $\psi_p(\mathbf{r})$ is the wave function of positron, $\psi_j(\mathbf{r})$ is the wave-function of electron on orbital j. For LDA, $\gamma_j = \lambda_j^{LDA}/\lambda_j^{IPM}$, where

$$\lambda_j^{LDA} = \pi r_e^2 c \int d\mathbf{r} n_j(\mathbf{r}) n_p(\mathbf{r}) \gamma(n_e(\mathbf{r})), \quad (5)$$

and λ_j^{IPM} is the annihilation rate calculated in the same way by independent-particle model (IPM), in which $\gamma \equiv 1$. For WDA, $\gamma_j = \lambda_j^{WDA}/\lambda_j^{IPM}$, where

$$\lambda_j^{WDA} = \pi r_e^2 c \int d\mathbf{r} n_j(\mathbf{r}) n_p(\mathbf{r}) \gamma(\tilde{n}_e(\mathbf{r})). \quad (6)$$

It is noteworthy that the shell partitioning method is also used here. The effective electron density $\tilde{n}_e(\mathbf{r})$ is used to evaluate the enhancement factor.

All computed Doppler spectra were convoluted with a Gaussian function with a FWHM corresponding to the experimental resolution (4.89×10^{-3} m_0c) as detailed in Section 2.2.

We have checked that the positron lifetimes and momentum distributions in lattice and single vacancy are similar with the results which were calculated in $4 \times 4 \times 4$ supercells with 520 eV energy cutoff and $4 \times 4 \times 4$ Γ-centered k-point mesh. Hence, we conclude that the 230 eV cutoff energy is a reasonable choice to calculate positron lifetimes and momentum distributions in tungsten.

2.2. Experimental methods

The materials used in this work are high purity (99.95 wt.%) polycrystalline tungsten slabs ($7 \times 7 \times 0.15$ mm^3). They were purchased from Goodfellow or supplied by EFDA. The samples were mechanically polished and annealed at least at 1600 °C during 1 h under vacuum ($< 10^{-7}$ mbar) to remove possible native and polishing induced defects. The prepared samples were characterized using PAS with different set-ups: A Doppler broadening spectrometer (DBS) and two types of positron annihilation lifetime spectrometers (PALS). At CEMHTI a Doppler Broadening Spectrometer coupled to a slow positron accelerator was used to characterize the sample close to the surface [11]. The positrons are naturally emitted from a ^{22}Na source, moderated by a tungsten foil and re-accelerated, guided by an electric and magnetic field, respectively. This instrument provides a variable monoenergetic positron beam, ranging from 0.5 to 25 keV, which is capable to probe as far as 700 nm in tungsten. The implanted positrons loose essentially all of their kinetic energy up to thermalization, then diffuse before annihilating with an electron of the matrix. The annihilated e^+-e^- pairs emit mostly two γ-rays with an energy of 511 $\pm$ ΔE keV. ΔE is the energy shift of one of the emitted photons which is proportional to the kinetic momentum of the e^+- e^- pairs in the propagating direction of the 511 keV photon, at the origin of Doppler broadening (DB) of the annihilation line centered at 511 keV. The DB spectrum is the distribution of the photon counts as a function of the kinetic momentum of the annihilated e^+- e^- pairs. The annihilation of e^+-e^- pairs is affected by the local electronic density. In DBS coupled with a slow positron beam, the DB spectrum is recorded as a function of positron energy E using a high purity germanium detector with about 10% dead time and ~1.25 keV energy resolution (full width at half maximum, FWHM). This energy resolution corresponds to a momentum resolution of 4.89×10^{-3} m_0c (m_0: electron mass, c: light speed). The detection efficiency of the γ-rays is higher than 25% at 1.33 MeV. As a positive charge, the positron is more favorable to be trapped at sites where the Coulomb repulsion of positive nuclei is smaller, such as vacancy-type defects. Once the positron is trapped, it annihilates with a surrounding electron in the vicinity of this localized trap. It is evident that the positron annihilation characteristics differ from one defect to another, therefore, PAS is a sensitive technique to the concentration and nature of the defects. In general, we identify the different annihilation characteristics as the shape parameter *(S)* and the wing parameter *(W)*, which correspond respectively to the ratio of the counts at low momentum and high momentum over the total count of the region of interest. It should be noted that these two parameters give only a relative comparison. In this work, the momentum ranges for the calculation of S and W were 0 - $|2.64| \times 10^{-3}$ m_0c and $(|9.80|$ - $|24.88|) \times 10^{-3}$ m_0c, respectively.

The experimental DBS results (the S and W values as a function of the positron incident energy, *S(E)* and *W(E)* curves) can be fitted by the program VEPFIT [39,40], with which the sample is decomposed into several layers. Each layer is assumed to be homogenous presenting the specific annihilation characteristics e.g. S, W and the effective diffusion length L_{eff}^+ and a thickness. These characteristics allow to recognize the defect distribution in the sample.

It should be noticed that up to 8 samples can be mounted on the sample holder and characterized in the same measurement campaign. Among them a UO_2 reference sample is used to check the proper operation of both the positron accelerator and the DB spectrometer. To compare the S and W results from one campaign to another, the S and W values are usually normalized to the ones of the UO_2 reference sample, and the normalized values of S and W are usually reported in our publications. In this paper, because the main objective is to compare the experimental data with the theoretical results, we checked that the S and W results for UO_2 reference are the same for all the measurements presented here and we reported the raw (not-normalized) values of S and W.

Positron lifetime was measured in thick pristine samples using a classical fast coincidence spectrometer and fast positrons directly emitted from a ^{22}Na source encapsulated in 6 µm aluminum foil. The source is sandwiched by two equivalent samples. The event count of the birth and the annihilation photons was collected by two detectors in coincidence. The time resolution of the spectrometer (full width at half maximum, FWHM) is about 212 ps. The ANAPC program was employed to fit the lifetime spectra with three source corrections in which the fixed first one is 230 ps with an intensity of about 23.59% which was calculated by using Bertolaccini formula [41], and two adjustable ones at 450 ps and 1500 ps with intensities of ~1.3 ± 0.3% and ~0.35 ± 0.05% respectively. To obtain more information on the ion-induced vacancy-type defects in the slow positron sensible region (0–700 nm), the positron lifetime was measured with a Pulsed Low Energy Positron Beam System (PLEPS) implemented at the NEutron-induced POsitron source at MUniCh (NEPOMUC) [12,13]. The time resolution (FWHM) was 280 ps with a count rate around 10^{-4} cts.s^{-1}. The spectra were fitted by the POSFIT program [42].

In the two fitting programs ANAPC and POSFIT, the lifetime spectrum $N(t)$ is considered as a convolution of the sum of exponential lifetime components τ_i weighted to their respective intensities I_i and the resolution of the measurement system $R(t)$ [43] after substracting the background noise (BG) of measurement.

$$\boldsymbol{N(t) = R(t) \otimes \sum \frac{I_i}{\tau_i} e^{-\frac{t}{\tau_i}} + BG}, \quad (7)$$

The average lifetime can be calculated as $\tau_{av} = \sum_i^I \tau_i$. Each spectrum contains a total count superior to 2×10^6 events of two types of measurement in order to ensure an accurate statistic.

The detailed experimental results are discussed in the Appendix.

3. Results and discussion

3.1. Positron lifetimes in vacancy clusters

The calculated lattice constant of tungsten is 3.182 Å, which is in good agreement with the experimental value, 3.16 Å [44]. The positron lifetimes obtained with LDA and WDA are listed in Table 1. Our LDA results show good agreement with the experimental results and reference calculations. However, the situation is more complicated for WDA. This is mainly due to the screening charge Q, a material-dependent phenomenological parameter, which plays an important role in correctly reproducing experimental positron lifetimes [24,29]. According to Callewaert et al. [24], Q is the scaling parameter of electron densities in WDA. The densities of valence electrons are scaled via the adjustment of the Q value. Setting $Q=1$ means no scaling is applied and this is consistent with the original WDA construction for surface states [27]. Increasing Q means decreasing the effective electron density, leading to the accumulation of more charge in the screening cloud. This would result in an increase of the annihilation rate and a decrease of positron lifetimes. Our calculations give results which are consistent with such an explanation. According to Ref. [24], different Q values should be used on different materials to obtain correct positron lifetimes. $Q=1.33$ was recommended for tungsten [24]. This is, however, only true in tungsten lattice and not necessarily appropriate for vacancies and vacancy clusters, as we show here. In this work, the calculated positron lifetime of the tungsten lattice is 107 ps when $Q=1.33$. This result is in good agreement with theoretical and experimental results. However, for the single vacancy, the calculated positron lifetime is 216 ps, which is significantly higher than the reference values (190–200 ps, theoretical and experimental values). This means that the recommended reference value, $Q=1.33$, is not fully proper to apply for calculations of positron lifetimes in defects. To find the most proper Q value, we compared positron lifetimes obtained with different Q values. When $Q=1$, positron lifetimes are significantly overestimated; when $Q=1.33$, WDA predicts the correct lifetime of tungsten lattice but an overestimated lifetime of the single vacancy. We finally found that $Q=1.6$ is a suitable value to get reasonable positron lifetimes. Compared with LDA results, $Q=1.6$ WDA yields similar positron lifetimes for both tungsten lattice and the single vacancy; and the lifetime saturates at large clusters limit with the value of ~450 ps. In Table 1, positron lifetimes with $Q=1.6$ shows an overall excellent agreement with both experimental and LDA values. Therefore, we conclude that, when using WDA, $Q=1.6$ should be used to correctly calculate positron lifetimes in tungsten.

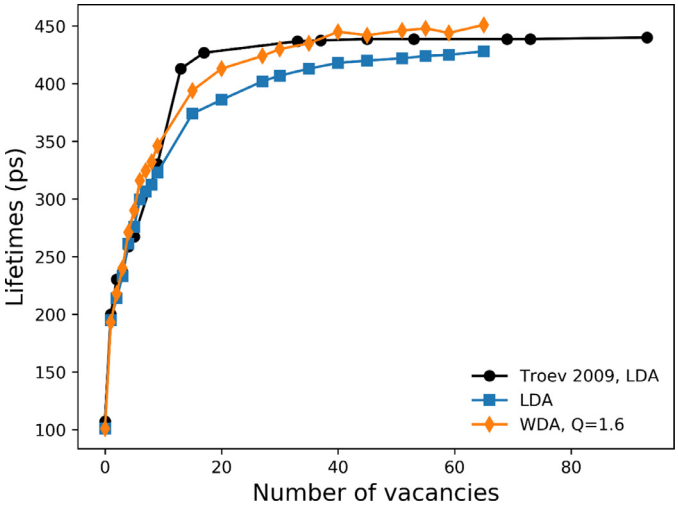

Fig. 1. Comparison of positron lifetimes between LDA, WDA with $Q=1.6$ and simulation results of Troev et al. [16].

In Fig. 1, we also compared our calculated positron lifetimes with the theoretical work from Troev et al. [16] in which the positron lifetimes were calculated with the LDA correlation potential and enhancement factor. For WDA, there is a slight fluctuation of lifetimes when there are more than 40 vacancies in a cluster. Such fluctuation is not observed in LDA results or in Ref. [16]. Since this fluctuation does not affect the overall trend, we suggest that it is insignificant. While different computational methods yield different positron lifetimes, their overall trends are the same. Firstly, the vacancy lifetimes increase rapidly with the increasing size of vacancy clusters; then, the vacancy lifetimes saturate between ~400–450 ps for big vacancy clusters. In both Table 1 and Fig. 1, our calculations, using both LDA and WDA, exhibit excellent agreement with both experimental and theoretical references. Because both LDA and WDA yield similar positron lifetimes, it seems that they both can correctly describe the positron-electron correlation potential in vacancy clusters. However, the computational

Table 1
Comparison of lifetimes given in ps between literature, LDA, WDA with Q values. $Q=1.33$ is the recommended value from Ref. [24].

	LDA	WDA, $Q=1.6$	WDA, $Q=1.33$	WDA, $Q=1$		Experiment
Lattice	101, 101[a], 108[b]	101	107, ~105[c]	117	Lattice	104 (this work), 102[d], 105[e]
Single vacancy	195, 193[a], 200[b]	193	216	250	Single vacancy	180[f], 200[g]
V_2	214, 226[a], 230[b]	218		284		
V_3	233, 237[b]	240		319		
V_4	261, 258[b]	271		376		
V_9	323, 330[b]	346		534		
V_{15}	374	394		689		
V_{27}	402	424		814		
V_{51}	422	446		951	Cavity*	375–424[h], 500[i]

[a] Reference [14].
[b] Reference [16].
[c] Reference [24].
[d] Reference [45].
[e] Reference [46].
[f] Reference [47].
[g] Reference [48].
[h] Reference [49].
[i] Reference [9].
* In many experiments, the estimated cluster sizes were based on the LDA theoretical calculations in Ref. [16]. But the saturated positron lifetime is usually around 400–500 ps, which is well-determined.

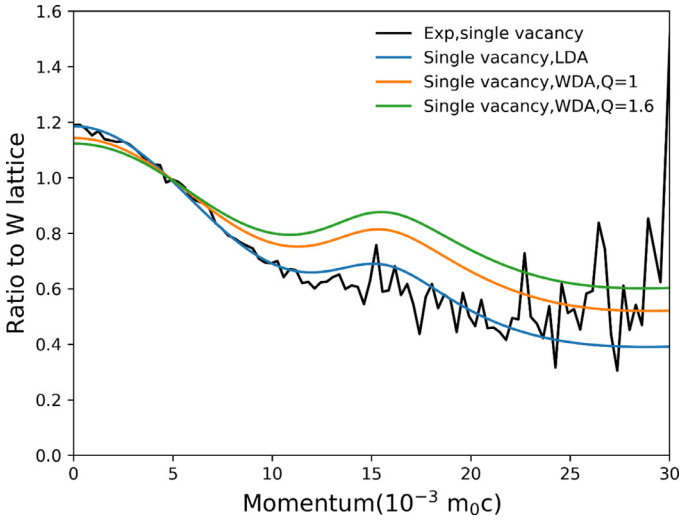

Fig. 2. Experimental and computed Doppler spectra for single vacancies in tungsten. The methodology used to obtain the experimental data of single vacancy is explained in the Appendix. The computational curves are convoluted with a Gaussian function with a FWHM of 4.89×10^{-3} m_0c.

Doppler spectra obtained with the two methods are quite different. We will discuss the Doppler spectra obtained with both methods in the following section.

3.2. Doppler spectra in vacancy clusters

Positron lifetimes alone are generally not enough to fully determine what type of defects we can find in materials. The lifetimes are quite strongly affected by the available open volume but not so sensitive to the chemistry of the atoms in the vicinity of the open volume. Therefore, we also calculated Doppler broadening spectra of vacancy clusters using LDA and WDA and we here discuss their differences. For WDA, we computed Doppler spectra using $Q = 1$ and 1.6.

Fig. 2 illustrates the Doppler spectra for a single vacancy obtained from experiment [48], and calculated using LDA and WDA. They are displayed as ratio curves where the Doppler spectra of defects are divided by the spectra of the tungsten lattice. The experimental data are determined as explained in Appendix. All theoretical curves show similar shape with the experimental result. Both LDA and WDA results have two peaks centered at 0 and $\sim 15 \times 10^{-3}$ m_0c. Compared with WDA, LDA shows in general better agreement with the experimental result in the full momentum range. For WDA, the agreement with the experimental curve is also good at low momentum ($< 10 \times 10^{-3}$ m_0c), but WDA tends to overestimate somewhat the intensity at high momentum ($> 10 \times 10^{-3}$ m_0c) both for the individual vacancy/lattice spectra (not shown) and their ratio, particularly with $Q = 1.6$. The difference between LDA and WDA is expected. LDA has been widely applied in numerous studies [7] and it has been shown that it generally yields reasonably accurate results for many materials.

Fig. 3 demonstrates the computed ratio curves of vacancy clusters using LDA. The experimental V_1 and V_N curves are also included (V_N corresponds to largest detectable vacancy cluster, see details in Appendix). In Fig. 3a, from V_1 to V_{15}, the intensities in the low momentum part increase and the high momentum part ($\sim 15 \times 10^{-3}$ m_0c) decrease with growing cluster size (illustrated with low momentum (LM) and high momentum (HM) arrows). This trend is the same as that found in experiments. Moreover, the theoretical V_{15} curve is also in good agreement with the experimental V_N curve. Nevertheless, a peculiar behavior is depicted in the ratio curves for larger vacancy clusters. In Fig. 3b for clusters from V_{20} to V_{65}, in contradiction with the experimental observation, the LDA predictions fail to satisfactorily capture the experimental evolution with respect to cluster size. The earlier growth trend is reversed and intensities in the low momentum part decrease while the high momentum part increases with growing cluster size (also illustrated with LM and HM arrows). This is clearly unreasonable and we must conclude that LDA is not able to reliably predict the Doppler broadening spectra for large vacancy clusters in tungsten.

The reason for the unusual behavior of the calculated momentum distribution of vacancy clusters is that LDA fails to correctly describe the electron-positron correlation potential and enhancement factor in large vacancy clusters, which are strongly inhomogeneous systems and involve non-local electron-positron correlations similarly to the case of positron-surface interactions. In Doppler broadening spectroscopy, valence electrons mainly contribute to the *S* parameter (low momentum range), while core electrons mainly contribute to the *W* parameter (high momentum range) [7]. For LDA, this is true for annihilation of positrons in the lattice state and trapped at small defects. However, for positron annihilation in large vacancy clusters, the weight of the valence electrons is strongly overestimated by LDA, as is clearly shown in Fig. 4. For tungsten lattice, valence electrons dominate at low momentum and core electrons dominate at high momentum. The gaps between core electron spectra and total spectra are quite narrow at high momentum. Nonetheless, for large vacancy cluster like V_{65}, LDA gives unreasonable results. For V_{65}, the gap between core and total spectrum is so wide that the valence electrons always dominate at all momentum ranges. Such unreasonably high contribution of valence electrons makes the Doppler spectra of large vacancy clusters physically unrealistic. Therefore, while LDA yields correct positron lifetimes and gives correct Doppler spectra for annihilation in the lattice and small defects, it is problematic to calculate the Doppler spectra for large vacancy clusters, at least for tungsten.

Compared with LDA, the advantage of WDA is that, for positrons in the vacuum, it could correctly capture the effects of the screening cloud at the surface [24]. Large vacancy clusters also have large vacuum regions and inner surfaces. Hence, we used WDA to calculate Doppler spectra of vacancy clusters in tungsten. Two different screening charge values, $Q = 1$ and 1.6, are utilized.

The ratio curves of vacancy clusters obtained with WDA are illustrated in Fig. 5 together with the experimental curves. Although both Q values show good agreement with experimental results for the single vacancy, they exhibit totally different behaviors for vacancy clusters. While $Q = 1.6$ is a reasonable value to calculate positron lifetimes, it is an unreasonable choice to calculate Doppler spectra of vacancy clusters. There are two main problems with $Q = 1.6$. The first one is that the spectra saturate at very small cluster sizes. In Fig. 5b, the ratio curves of V_6 and V_{65} almost overlap with each other, implying full saturation already at V_6. Such saturation size is too small and unrealistic. The second problem is that the calculated ratio curves of vacancy clusters do not agree well with experimental results at any momentum range. For the single vacancy, there is a fair agreement between experimental and theoretical curves at low momentum. However, for big vacancy clusters, compared with the experimental curve, $Q = 1.6$ severely underestimates the intensity at low momentum and overestimates the intensity at high momentum. Therefore, $Q = 1.6$ should not be used to calculate Doppler spectra of vacancy clusters in tungsten, even though it was the most appropriate choice for WDA lifetime calculations.

Unlike the case of $Q = 1.6$, using $Q = 1$ yields too long and unrealistic positron lifetimes. It is, however, a much better choice to calculate Doppler spectra of vacancy clusters. In Fig. 5a, the

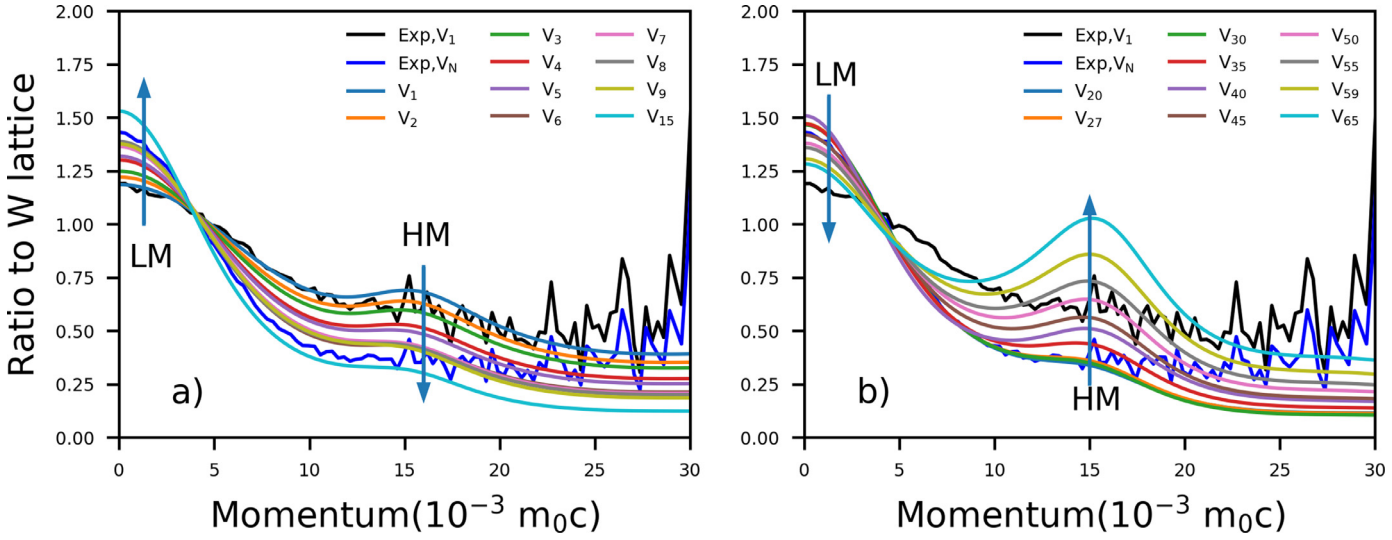

Fig. 3. Experimental and computed LDA Doppler spectra of vacancy clusters in tungsten. Ratio curves from V_1 to V_{65} are divided into two figures for clear presentation. The arrows in the figures show the evolution of the low momentum (LM) and high momentum (HM) parts with the growth of the clusters. The methodology used to obtain the experimental data of V_1 and V_N is explained in the Appendix. The computational curves are convoluted with a Gaussian function with a FWHM of 4.89×10^{-3} m_0c. a) The ratio curves from V_1 to V_{15}. b) The ratio curves from V_{20} to V_{65}.

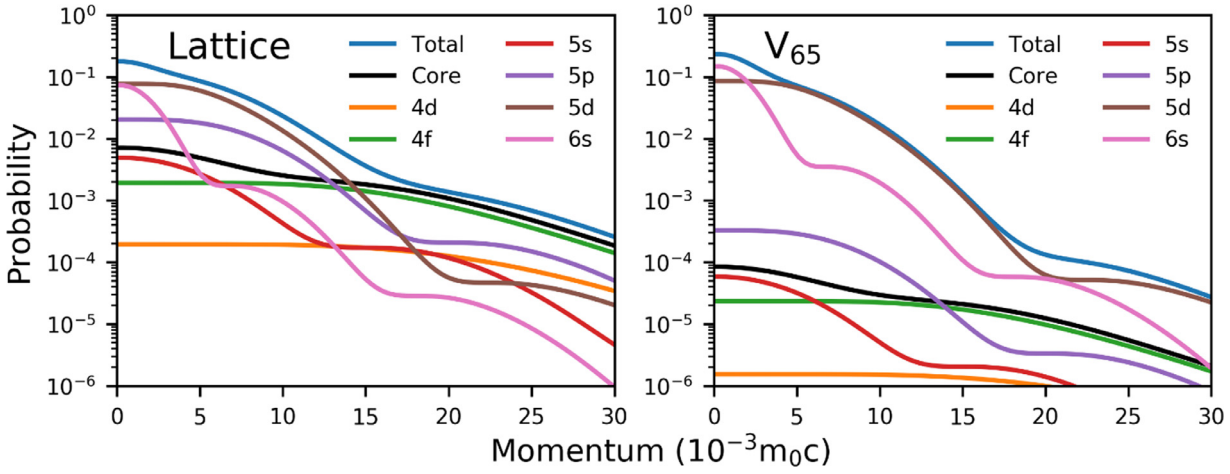

Fig. 4. LDA prediction of the individual contribution of the different electron shells involved in the positron annihilation. The results of tungsten lattice and V_{65} are shown. This was calculated by the atomic superposition method [50]. The core electron shells are explicitly shown. The 5p, 5d and 6 s electrons are viewed as valence electrons. The other electrons are considered core electrons. For core electrons, only 4d, 4f and 5 s electrons are presented because the contributions of other electrons are negligible.

difference between ratio curves of V_{15} and V_{65} is small, which means that the calculated Doppler spectra saturate when there are more than 15 vacancies. This is a reasonable saturation cluster size. Meanwhile, although $Q=1$ always overestimates the intensities at high momentum, the calculated ratio curves of the single vacancy and vacancy clusters still show fair agreement with experimental results in the low momentum range. Hence, Fig. 5 indicates that WDA with $Q=1$, the default value in the original WDA model [27], is a suitable option to calculate Doppler spectra of vacancy clusters in tungsten. It is noteworthy that we also performed tests to calculate the momentum distribution by using the WDA correlation potential combined with the LDA enhancement (not shown). Similar behavior as in LDA also appeared in the curves. Therefore, it is important to always use the WDA enhancement.

Based on WDA Doppler spectra with $Q=1$, we calculated S and W parameters of vacancy clusters in tungsten. The results are presented in Fig. 6. In Fig. 6a, the S and W parameters are presented as relative parameters divided by tungsten lattice values. It shows a clear trend that S parameter increases, and W parameter decreases with the vacancy cluster size until 15 vacancies. For clusters with more than 15 vacancies, the cluster sizes do not have significant effect on S and W parameters. The (S, W) points of V_{15} and V_{65} are rather close to each other. All vacancy clusters points are roughly located on the dashed black line D_N. Fig. 6b presents the experimental (S, W) points of tungsten lattice, single vacancy and the vacancy cluster V_N with (S_{max}, W_{min}), where the S and W parameters are listed in Table 2 in Appendix. The theoretical results in Fig. 6a clearly show the same trend as the experimental results in Fig. 6b. This indicate that even though WDA overestimates the intensities at high momentum, it correctly captures the saturation trend and is a suitable method to calculate the Doppler spectra of vacancy clusters in tungsten.

Since vacancy clusters in Fig. 6a are on the dashed black line D_N from single vacancy to V_{65}, we also present the projected fraction on the D_N dashed line as a function of the size of vacancy clusters. Here the projected fraction was calculated by the following steps. Firstly, each point of vacancy clusters was projected on the D_N dashed line in Fig. 6a. Then, the projected fraction can be obtained by calculating the distance to the single vacancy divided by the length of the D_N dashed line. Fig. 7 shows the result. It is

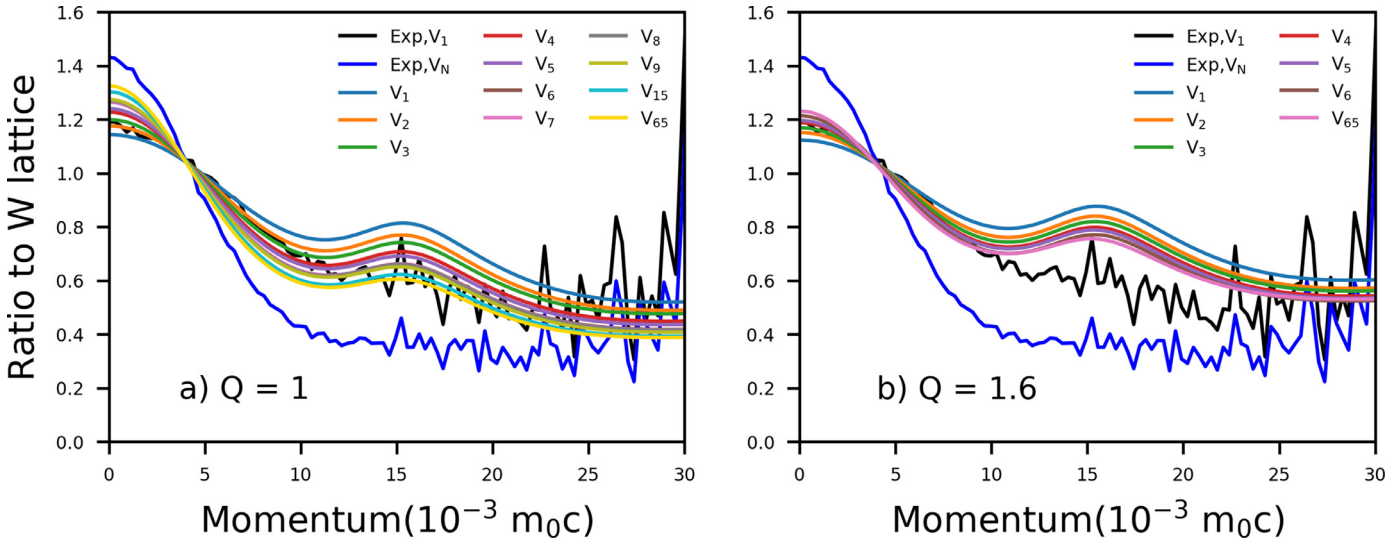

Fig. 5. Experimental and computed WDA Doppler spectra of vacancy clusters in tungsten. Two Q values, 1 and 1.6, are used. For $Q=1$, ratio curves between V_{15} and V_{65} are not shown; for $Q=1.6$, ratio curves between V_6 and V_{65} are not shown. This is because they are almost perfectly overlapping with each other. The methodology used to obtain the experimental data of V_1 and V_N is explained in the Appendix. The computational curves are convoluted with a Gaussian function with a FWHM of 4.89×10^{-3} m_0c.

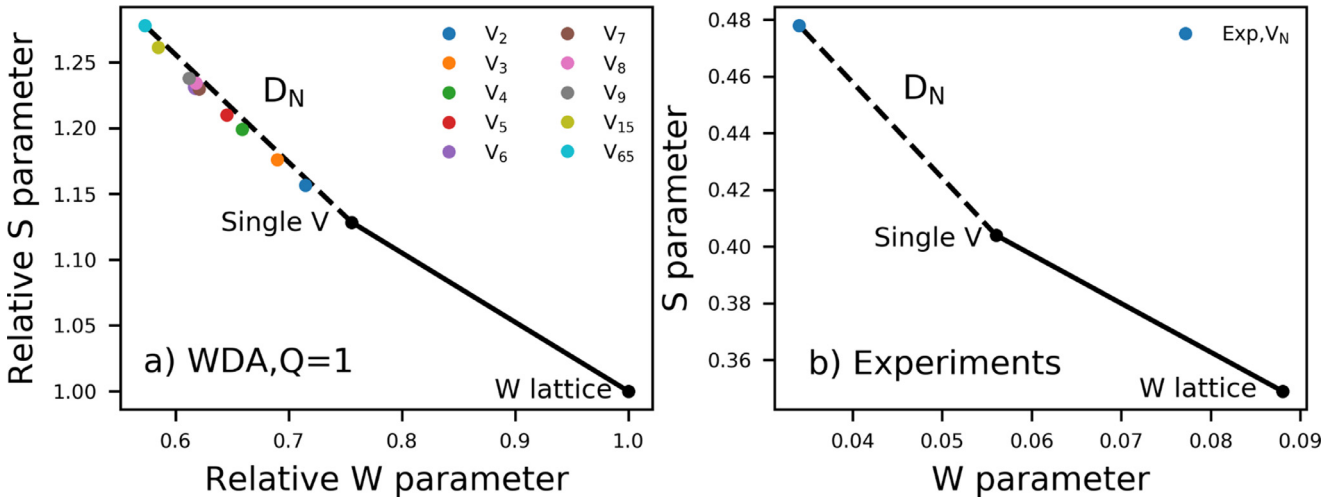

Fig. 6. a) The computed S and W parameters calculated from Doppler spectra with WDA, $Q=1$. b) The experimental S and W parameters for tungsten lattice, single vacancy and V_N. The experimental S and W values are taken from Table 2. The methodology used to obtain the experimental data is explained in the Appendix. In both figures, D_N refers to the black dashed lines.

Table 2
The S and W parameters for the pristine sample, single vacancy (V_1) and that of the largest detected vacancy cluster (V_N) as extracted from the DB measurements with error bars. The methodology used to obtain the experimental data is explained in the Appendix.

	S	W
Pristine sample or extrapolated perfect ***lattice***	0.349 ± 0.004	0.088 ± 0.005
V_1	0.404 ± 0.006	0.056 ± 0.002
V_N	0.478 ± 0.003	0.034 ± 0.001

clearly shown that the saturation happens for more than 15 vacancies. The shape of the curve is similar to the curve in Fig. 1, where the saturation of lifetimes also happens near 15 vacancies. The results in Fig. 7 can be used to interpret experimental results to determine the size of vacancy clusters if the (S, W) points are between V_1 and V_N.

In this study, we have found that LDA and WDA have completely different behavior for big vacancy clusters. Therefore, we also compared the positron densities obtained by both methods. The positron density in V_{65} can be viewed from the contour plot in Fig. 8. Both LDA and WDA results indicate that positrons are trapped at the V_{65} cluster. The LDA result illustrates that the center of the vacancy cluster has the highest positron density, similarly to other calculations [7,16]. However, the WDA predicts a significantly different distribution than that of LDA. The WDA results show that while positrons are trapped in the vacancy cluster, they do not tend to stay at the center. On the contrary, positrons tend to bind with the atoms at the inner surface of the vacancy cluster.

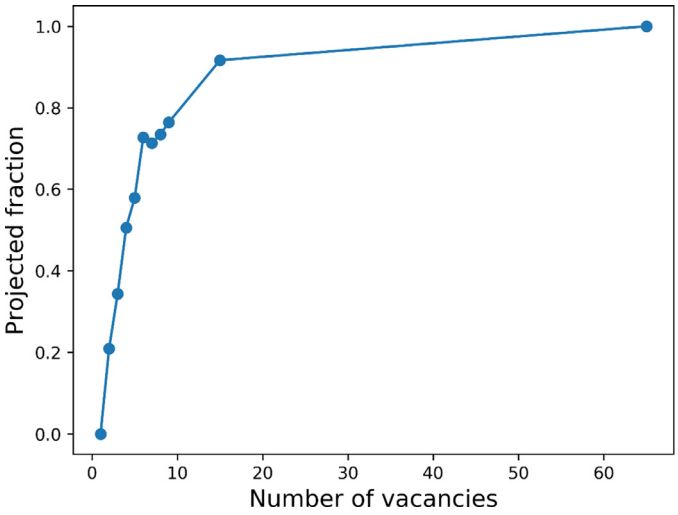

Fig. 7. Projected fraction as a function of the number of vacancies from V_1 to V_{65}.

The positron density near the surface is higher than at the center. As a result, a shell-like structure is shown in the WDA results. The WDA-calculated positron densities are expected to be more physically realistic. Experimental result [51] shows that the binding energy between positron and tungsten (111) surface is 2.81 eV. This indicates that positrons might bind with the inner surfaces of large vacancy clusters. Compared with $Q=1$, a higher Q value, $Q=1.6$, would lead to stronger binding to the surface and lower positron density at the center. Such stronger binding with surface atoms might result in higher annihilation rate and higher contribution of core electrons, which correlates better with the experimental results, as seen in the comparison of Fig. 3b and Fig 5a. For $Q=1.6$, the higher annihilation rate means shorter positron lifetimes. The higher contribution of core electrons means ratio curves would have higher intensity at high momentum range, as shown in Fig. 5b.

The breakdown of LDA in case of large vacancy clusters can be understood using these two if its features, 1) its complete locality or the lack of non-local correlations important for describing bound surface states, and 2) its built-in zero-electron-density limit corresponding to negative positronium ion formation (lifetime of 478 ps) in homogenous vacuum, which is not the physical case in real measurements of vacancy clusters. For defect-free W, monovacancy and smallest vacancy clusters the LDA is physically valid. Even though the LDA lifetime appears to saturate at a reasonable value as a function of cluster size, this is only coincidence and the physical mechanism behind is not correct.

4. Conclusion

In this paper, we present a systematic theoretical work compared to experimental results to study vacancy defects in tungsten. We demonstrate that the vacancy defect sizes can be estimated by combining theoretical and experimental results. The experimental results demonstrate a clear trend of the (S, W) points from single vacancies to vacancy clusters V_N with (S_{max}, W_{min}). We calculated the positron lifetimes and Doppler spectra in tungsten by both LDA and WDA methods. We clearly show the respective advantages and disadvantages of LDA and WDA. For LDA, the calculated lifetimes have good agreement with other experimental and theoretical references. However, when calculating the Doppler spectra, LDA cannot satisfactorily reproduce the experimental evolution with the vacancy cluster size. This is because LDA fails to correctly describe the electron-positron correlation potential and non-local correlations in inhomogeneous systems, such as large vacancy clusters and surfaces. There is a clear "failure" point for LDA at V_{15}. From V_1 to V_{15}, the calculated curves have the same trend as in experiments. When there are more than 15 vacancies, LDA fails to yield the correct trend. For WDA, the value of the phenomenological parameter, the screening charge Q, is a vital component in yielding reliable results. Different Q values should be used for different calculations, like $Q=1.6$ for accurate positron lifetimes while $Q=1$ for good Doppler spectra. We show that the earlier proposed $Q=1.33$ is only applicable for lattice calculations and not for predicting vacancy properties. The absolute agreement of the WDA Doppler spectra with the experimental results is not very good. But the trend given by WDA is in excellent agreement with the experimental results. Furthermore, WDA also predicted the binding between positron and W surface, which agrees well with experimental observation. Based on these findings, we conclude that it is important to select an appropriate method for the property one is interested in predicting, and that for experimental (S, W) Doppler broadening characterization of vacancy clusters in tungsten, WDA is a more appropriate choice than LDA. This may well prove to be true also in other metallic materials.

Declaration of Competing Interest

The authors declare that they have no known competing financial interests or personal relationships that could have appeared to influence the work reported in this paper.

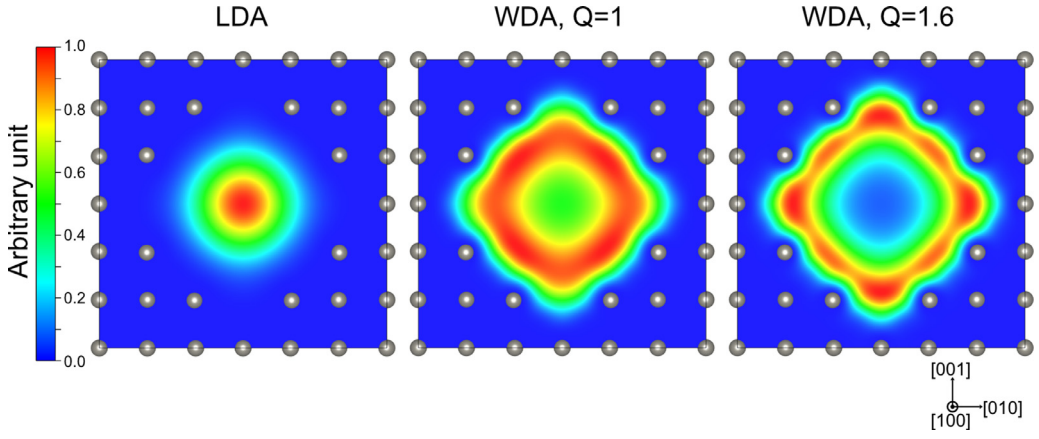

Fig. 8. Contour plots of the positron density at the cross section of a (100) plane for the V_{65} system.

CRediT authorship contribution statement

Qigui Yang: Formal analysis, Software, Writing – original draft, Writing – review & editing. **Zhiwei Hu:** Formal analysis, Investigation, Validation, Writing – original draft, Writing – review & editing. **Ilja Makkonen:** Software, Writing – review & editing. **Pierre Desgardin:** Investigation, Supervision. **Werner Egger:** Investigation, Formal analysis. **Marie-France Barthe:** Conceptualization, Supervision, Writing – review & editing. **Pär Olsson:** Conceptualization, Supervision, Writing – review & editing.

Data Availability

Data will be made available on request.

Acknowledgement

This work has been carried out within the framework of the EUROfusion Consortium, funded by the European Union via the Euratom Research and Training Programme (Grant Agreement No 101052200 — EUROfusion). Pär Olsson acknowledges funding from the Euratom research and training program 2019–2020 under grant agreement No 900018 (ENTENTE project). Views and opinions expressed are however those of the authors only and do not necessarily reflect those of the European Union or the European Commission. Neither the European Union nor the European Commission can be held responsible for them. Qigui Yang acknowledges the financial support by the China Scholarship Council (No. 201807930008) and Svensk Kärnbränslehantering AB. Ilja Makkonen acknowledges financial support from the Academy of Finland (Grants No. 285809, 293932, 319178, 334706, and 334707). The computational resources were provided by the Swedish National Infrastructure for Computing (SNIC) and by the CINECA HPC center in Italy. The authors gratefully thank Vincent Callewaert for helpful discussions.

Appendix. Detailed experimental results

Pristine and damaged tungsten samples were characterized using PAS. Fig. 9a shows the normalized positron lifetime spectra obtained from pulsed and conventional spectrometer for a ^{3}He-damaged sample containing 98% V_1 and a pristine one, respectively. Fig. 9b exhibits the low momentum parameter S as a function of the positron incident energy E, $S(E)$ of the pristine tungsten sample measured using Slow Positron Beam Doppler Broadening (SPB-DB). The $S(E)$ and $W(E)$ curves of the ^{3}He-damaged sample can be found in [48].

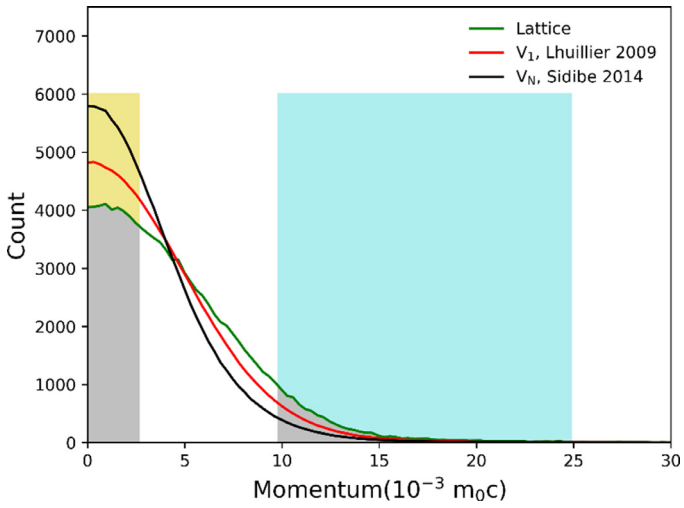

Fig. 10. The averaged DB spectrum from 6 to 25 keV for the largest vacancy cluster V_N and single vacancy V_1 in comparison with that of pristine one obtained for 25 keV slow positron. The windows for line-shape parameters S an W are also illustrated. The V_1 and V_N curves are from Ref. [48] and Ref. [52], respectively.

Fig. 10 illustrates the DB spectra of two damaged tungsten samples in which the annihilation characteristics were identified in previous works [48,52] as V_1 and vacancy clusters V_N and the pristine sample corresponding to Fig. 9b which has the lattice characteristics.

The positron lifetime measurement in pristine samples were carried out with classical fast positron 'sandwich' configuration which penetrates at most 50 μm in tungsten as calculated with the reported equation by Dryzek et al. [53].. Only one lifetime component was extracted in pristine samples at about 103.8 ± 0.3 ps, a similar value to that reported ones [54,55]. That indicates a quite low defect concentration in the pristine samples (Fig. 9a).

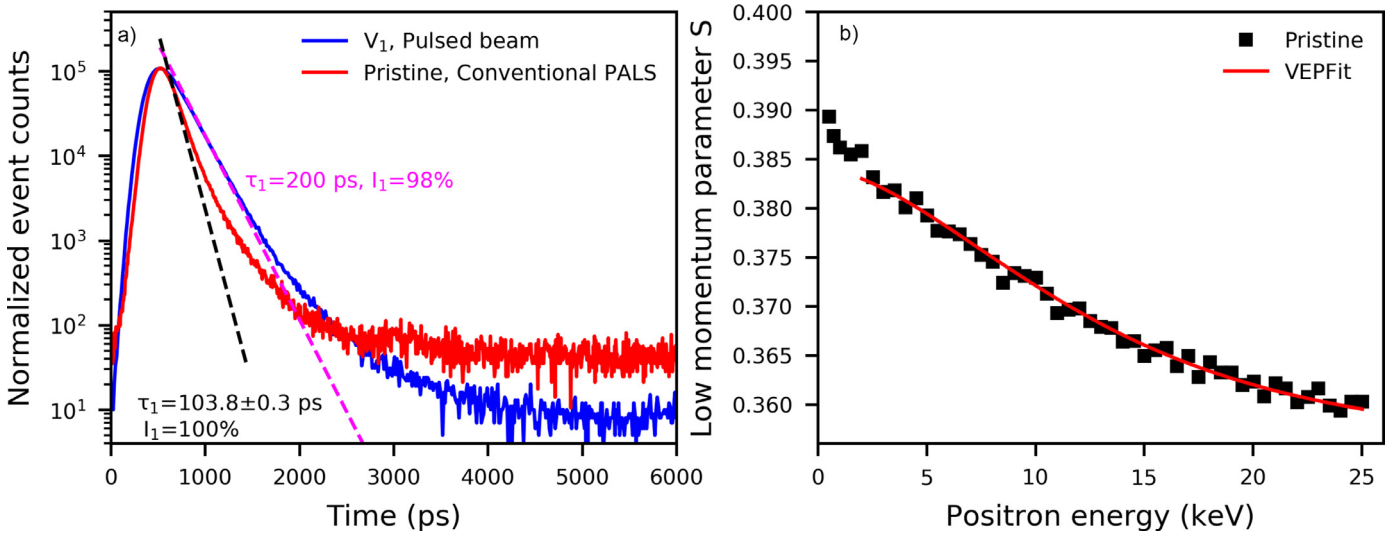

Fig. 9. a) PALS spectrum of one pristine sample obtained from the conventional measurement (with an order of magnitude higher background noise that Pulsed beam measurement and ~75% annihilations occurs in the samples) in comparison with confirmed single vacancy V_1 one acquired from pulsed beam and b) the parameter S as a function of the incident energy for one pristine sample extracted from SPB-DB measurements.

Fig. 9b shows the low momentum annihilation fraction S as a function of positron energy E in pristine tungsten samples. It should be pointed out that the $W(E)$ curve is the reverse of the $S(E)$ and consequently it is not shown in Fig. 9. S decreases slowly (and W respectively increases) while the positron energy increases. It indicates that a considerable fraction of positrons diffuses back to the surface. The $S(E)$ and $W(E)$ curves were fitted using the VEPFIT program considering only one homogeneous layer that can be considered as the bulk of the sample. The annihilation characteristics S and W in the bulk are respectively $S = 0.355 \pm 0.003$ and $W = 0.096 \pm 0.0003$. If we normalize these values to compare them with our previous results already published, we obtain $S_{norm} = 0.367 \pm 0.003$ and $W_{norm} = 0.085 \pm 0.001$.These values are very close to the ones determined for positron annihilation in the tungsten lattice [48]. The effective diffusion length in the bulk is $131 \pm 5nm$. This value is within the range reported in the literature (between 80 and 140 nm) [56] for intrinsic diffusion length of positrons in polycrystalline tungsten with a purity of 99.95%.wt. It confirms that the defect concentration in the pristine sample is very low and that the sample can be considered as perfect lattice for positron spectroscopy as concluded from PALS results. Thus, in the measured positron energy range (from 0.5 to 25 keV), the annihilation occurs both in the perfect lattice and at the surface of the sample with a fraction of annihilation at the surface which decreases while positron energy increases and that becomes the lowest at the highest energy of 25 keV.

So we can express $S(E)$ as follows

$$S(E) = f_{surf}(E) \times S_{surf} + f_L(E) \times S_L, \tag{8}$$

where $f_{surf}(E)$ and $f_L(E)$ are respectively the fractions of positrons annihilated at the surface and in the lattice and S_{surf} and S_L the positron annihilation characteristics of surface and lattice, respectively. Moreover, because all positrons annihilate at the end, we can also write that

$$f_{surf}(E) + f_L(E) = 1. \tag{9}$$

So the fraction of positrons annihilated at the surface for the highest energy (25 keV) can be estimated at 17% in contrast to the value obtained for the lowest one (2 keV) which reaches 97%. It means that there is still a low contribution of positron annihilation at the surface in the DB spectrum measured at 25 keV and that of 2 keV could be considered as surface contribution. Then, we could extract the DB_L spectrum of tungsten lattice, via the following expression:

$$\mathrm{DB}(25\ \mathrm{keV}) = f_{surf}(25\ \mathrm{keV}) \times DB(2\ \mathrm{keV}) + f_L(25\ \mathrm{keV}) \times\ \mathrm{DB}_L. \tag{10}$$

This spectrum will be considered as the momentum distribution of e^+-e^- annihilated pairs which is the closest of the perfect lattice one and is plotted in Fig. 10.

Lhuillier et al. Debelle et al. [48,8] employed SPB-DB spectroscopy and demonstrated that the concentration of the ^{3}He-induced vacancy-type defects in tungsten saturated at room temperature, once the fluence reaches about 5×10^{16} cm^{-2}. The nature of induced defects was identified by PALS using PLEPS setup. One lifetime component of 200 ps with an intensity of 98% was extracted by the POSFIT program, (the lifetime spectrum is reported in Fig. 9a. This lifetime value has been compared to the calculated [15,16,57] and experimental ones [47,58,59] and attributed to annihilation at single vacancy. The right side of the Doppler broadening spectrum reported in Fig. 10 as representing the single vacancy annihilation state is an average of several ones measured in the energy range from 6 to 25 keV, between which the value $S(E)$ and $W(E)$ exhibit a plateau and this range includes the one as for the PALS measurement (14 keV).

In our previous works [52], we employed slow positron beam Doppler Broadening spectroscopy (SPB-DB) to investigate the radiation-induced vacancy-type defects in the self-irradiated polycrystalline tungsten slabs. The irradiations were carried out at low temperature (−185 K) with an energy of 20 MeV and a fluence of about 3.7×10^{14} cm^{-2}. According to the Kinchin-Pease (K-P) formalism of the Stopping and Range of Ions in Matter (SRIM [60]) program using a displacement threshold energy $E_d = 55.3$ eV for tungsten [61], the damage dose corresponds to 1 dpa for giving fluence in the probed depth of the SPB-DB spectroscopy (~700 nm). After irradiations, the self-irradiated samples were isochronally annealed from 150 to 1400 °C during 1 h, the evolution of vacancy-type defects was monitored by SPB-DB measurement for each annealing temperatures [52]. When annealing temperature increases from 150 to 450 °C, between which the migration of the single vacancies was confirmed [8], the single vacancies migrate and probably meet and coalesce each other or integrate in small clusters leading to a growth up of the mean clusters' size. Practically, the value of the S increases and W decreases until 500 °C signifying the agglomeration of the single vacancies and small clusters. The S and W parameters do not evolve for the temperatures ranging from 550 to 850 °C. From 900 to 1400 °C, with increasing temperature, the S decreases and W increases and tend the S-W values of the pristine sample [52]. These results indicate a saturation of the defects with some specific values ($S_{\max}$, $W_{\min}$) between 500 and 850 °C. At over 900 °C, the recovery mechanism initiates, a similar process was observed by Ferroni et al. [62] in self-irradiated tungsten. These ($S_{\max}$, $W_{\min}$) values probably correspond to the largest clusters detectable in our SPB-DB experiments performed in tungsten (see Ref. [10]).

Fig. 10 shows also the average of the right side of the DB spectrum obtained in the self-irradiated sample (1 dpa) after sequential 1h-annealing until 550 °C for the positron energy spanning from 8 to 25 keV, between which the value $S(E)$ and $W(E)$ exhibit a plateau [52,56].

As expected, the momentum distribution of annihilated pairs is clearly narrower for vacancy defects in comparison with perfect lattice and for vacancy clusters V_N in comparison with single vacancy V_1.

In the following, contrary to what is done classically, the S and W values are extracted from only the right side of the DB spectrum. Because of the Compton effect, the background is higher at left side of a classic experimental DB spectrum. Although this effect was considered when removing the background, the right side of the DB spectrum is the most proper to compare to the theoretical momentum distributions. Table 2 summarizes the S and W values extracted from the right-side of the DB spectra as illustrated in Fig. 10, of pristine sample (close to perfect lattice spectrum), single vacancy (V_1) and the largest vacancy cluster (V_N).

References

[1] J. Marian, C.S. Becquart, C. Domain, S.L. Dudarev, M.R. Gilbert, R.J. Kurtz, D.R. Mason, K. Nordlund, A.E. Sand, L.L. Snead, T. Suzudo, B.D. Wirth, Recent advances in modeling and simulation of the exposure and response of tungsten to fusion energy conditions, Nucl. Fusion 57 (2017) 092008, doi:10.1088/1741-4326/aa5e8d.

[2] S.J. Zinkle, L.L. Snead, Designing radiation resistance in materials for fusion energy, Annu. Rev. Mater. Res. 44 (2014) 241–267, doi:10.1146/annurev-matsci-070813-113627.

[3] X. Hu, T. Koyanagi, M. Fukuda, Y. Katoh, L.L. Snead, B.D. Wirth, Defect evolution in single crystalline tungsten following low temperature and low dose neutron irradiation, J. Nucl. Mater. 470 (2016) 278–289, doi:10.1016/j.jnucmat.2015.12.040.

[4] J. Fikar, R. Schäublin, Stability of small vacancy clusters in tungsten by molecular dynamics, Nucl. Instrum. Methods Phys. Res. Sect. B 464 (2020) 56–59, doi:10.1016/j.nimb.2019.11.044.

[5] D.R. Mason, D. Nguyen-Manh, C.S. Becquart, An empirical potential for simulating vacancy clusters in tungsten, J. Phys. Condens. Matter 29 (2017) 505501, doi:10.1088/1361-648X/aa9776.

[6] O. El-Atwani, E. Esquivel, M. Efe, E. Aydogan, Y.Q. Wang, E. Martinez, S.A. Maloy, Loop and void damage during heavy ion irradiation on nanocrystalline and coarse grained tungsten: microstructure, effect of dpa rate, temperature, and grain size, Acta Mater. 149 (2018) 206–219, doi:10.1016/j.actamat.2018.02.035.

[7] F. Tuomisto, I. Makkonen, Defect identification in semiconductors with positron annihilation: experiment and theory, Rev. Mod. Phys. 85 (2013) 1583–1631, doi:10.1103/RevModPhys.85.1583.

[8] A. Debelle, M.F. Barthe, T. Sauvage, First temperature stage evolution of irradiation-induced defects in tungsten studied by positron annihilation spectroscopy, J. Nucl. Mater. 376 (2008) 216–221, doi:10.1016/j.jnucmat.2008.03.002.

[9] M. Zibrov, W. Egger, J. Heikinheimo, M. Mayer, F. Tuomisto, Vacancy cluster growth and thermal recovery in hydrogen-irradiated tungsten, J. Nucl. Mater.. (n.d.). https://doi.org/10.1016/j.jnucmat.2020.152017.

[10] Z. Hu, P. Desgardin, C. Genevois, J. Joseph, B. Décamps, R. Schäublin, M.-.F. Barthe, Effect of purity on the vacancy defects induced in self–irradiated tungsten: a combination of PAS and TEM, J. Nucl. Mater. 556 (2021) 153175, doi:10.1016/j.jnucmat.2021.153175.

[11] P. Desgardin, L. Liszkay, M.F. Barthe, L. Henry, J. Briaud, M. Saillard, L. Lepolotec, C. Corbel, G. Blondiaux, A. Colder, P. Marie, M. Levalois, Slow Positron Beam Facility in Orléans, MSF 363–365 (2001) 523–525, doi:10.4028/www.scientific.net/MSF.363-365.523.

[12] W. Egger, P. Sperr, G. Kögel, G. Dollinger, Pulsed low energy positron system (PLEPS) at the Munich research reactor FRM II, Phys. Status Solidi (c) 4 (2007) 3969–3972, doi:10.1002/pssc.200675812.

[13] C. Hugenschmidt, G. Kögel, R. Repper, K. Schreckenbach, P. Sperr, B. Straßer, W. Triftshäuser, The neutron induced positron source at Munich – NEPOMUC, Nucl. Instrum. Methods Phys. Res. Sect. B 221 (2004) 160–164, doi:10.1016/j.nimb.2004.03.048.

[14] P. Staikov, N. Djourelov, Simulations of ⟨1 0 0⟩ edge and 1/2 ⟨1 1 1⟩ screw dislocations in α-iron and tungsten and positron lifetime calculations, Physica B 413 (2013) 59–63, doi:10.1016/j.physb.2012.12.026.

[15] A. Yabuuchi, M. Tanaka, A. Kinomura, Short positron lifetime at vacancies observed in electron-irradiated tungsten: experiments and first-principles calculations, J. Nucl. Mater. 542 (2020) 152473, doi:10.1016/j.jnucmat.2020.152473.

[16] T. Troev, E. Popov, P. Staikov, N. Nankov, T. Yoshiie, Positron simulations of defects in tungsten containing hydrogen and helium, Nuclear Instr. Methods Phys. Res., Sec. B 267 (2009) 535–541, doi:10.1016/j.nimb.2008.11.045.

[17] V.J. Ghosh, M. Alatalo, P. Asoka-Kumar, B. Nielsen, K.G. Lynn, A.C. Kruseman, P.E. Mijnarends, Calculation of the Doppler broadening of the electron-positron annihilation radiation in defect-free bulk materials, Phys. Rev. B 61 (2000) 10092, doi:10.1103/PhysRevB.61.10092.

[18] P. Asoka-Kumar, M. Alatalo, V.J. Ghosh, A.C. Kruseman, B. Nielsen, K.G. Lynn, Increased elemental specificity of positron annihilation spectra, Phys. Rev. Lett. 77 (1996) 2097–2100, doi:10.1103/PhysRevLett.77.2097.

[19] E. Boroński, R.M. Nieminen, Electron-positron density-functional theory, Phys. Rev. B 34 (1986) 3820–3831, doi:10.1103/PhysRevB.34.3820.

[20] J. Wiktor, G. Jomard, M. Torrent, M.-.F. Barthe, M. Bertolus, Fully self-consistent calculations of momentum distributions of annihilating electron-positron pairs in SiC, Phys. Rev. B. 93 (2016) 195207, doi:10.1103/PhysRevB.93.195207.

[21] J. Wiktor, M.-.F. Barthe, G. Jomard, M. Torrent, M. Freyss, M. Bertolus, Coupled experimental and DFT + U investigation of positron lifetimes in UO 2, Phys. Rev. B. 90 (2014) 184101, doi:10.1103/PhysRevB.90.184101.

[22] I. Makkonen, M. Hakala, M.J. Puska, Modeling the momentum distributions of annihilating electron-positron pairs in solids, Phys. Rev. B 73 (2006) 035103, doi:10.1103/PhysRevB.73.035103.

[23] P. Folegati, I. Makkonen, R. Ferragut, M.J. Puska, Analysis of electron-positron momentum spectra of metallic alloys as supported by first-principles calculations, Phys. Rev. B 75 (2007) 054201, doi:10.1103/PhysRevB.75.054201.

[24] V. Callewaert, R. Saniz, B. Barbiellini, A. Bansil, B. Partoens, Application of the weighted-density approximation to the accurate description of electron-positron correlation effects in materials, Phys. Rev. B 96 (2017) 1–13, doi:10.1103/PhysRevB.96.085135.

[25] O. Gunnarsson, M. Jonson, B.I. Lundqvist, Descriptions of exchange and correlation effects in inhomogeneous electron systems, Phys. Rev. B 20 (1979) 3136–3164, doi:10.1103/PhysRevB.20.3136.

[26] K.O. Jenson, A.B. Walker, Non-local positron-electron density functional theory and the positron surface state, J. Phys. F Met. Phys. 18 (1988) L277–L285, doi:10.1088/0305-4608/18/12/002.

[27] A. Rubaszek, Electron-positron enhancement factors at a metal surface: aluminum, Phys. Rev. B 44 (1991) 10857–10868, doi:10.1103/PhysRevB.44.10857.

[28] V.A. Chirayath, V. Callewaert, A.J. Fairchild, M.D. Chrysler, R.W. Gladen, A.D. McDonald, S.K. Imam, K. Shastry, A.R. Koymen, R. Saniz, B. Barbiellini, K. Rajeshwar, B. Partoens, A.H. Weiss, Auger electron emission initiated by the creation of valence-band holes in graphene by positron annihilation, Nat. Commun. 8 (2017) 1–7, doi:10.1038/ncomms16116.

[29] W. Shi, V. Callewaert, B. Barbiellini, R. Saniz, M. Butterling, W. Egger, M. Dickmann, C. Hugenschmidt, B. Shakeri, R.W. Meulenberg, E. Brück, B. Partoens, A. Bansil, S.W.H. Eijt, Nature of the positron state in CdSe quantum dots, Phys. Rev. Lett. 121 (2018) 57401, doi:10.1103/PhysRevLett.121.057401.

[30] G. Kresse, J. Furthmüller, Efficient iterative schemes for ab initio total-energy calculations using a plane-wave basis set, Phys. Rev. B 54 (1996) 11169–11186, doi:10.1103/PhysRevB.54.11169.

[31] P.E. Blöchl, Projector augmented-wave method, Phys. Rev. B 50 (1994) 17953–17979, doi:10.1103/PhysRevB.50.17953.

[32] J.P. Perdew, K. Burke, M. Ernzerhof, Generalized gradient approximation made simple, Phys. Rev. Lett. 77 (1996) 3865–3868, doi:10.1103/PhysRevLett.77.3865.

[33] J. Hou, Y.-.W. You, X.-.S. Kong, J. Song, C.S. Liu, Accurate prediction of vacancy cluster structures and energetics in bcc transition metals, Acta Mater 211 (2021) 116860, doi:10.1016/j.actamat.2021.116860.

[34] M.J. Puska, A.P. Seitsonen, R.M. Nieminen, Electron-positron Car-Parrinello methods: self-consistent treatment of charge densities and ionic relaxations, Phys. Rev. B 52 (1995) 10947–10961, doi:10.1103/PhysRevB.52.10947.

[35] N.D. Drummond, P. López Ríos, R.J. Needs, C.J. Pickard, Quantum Monte Carlo study of a positron in an electron gas, Phys. Rev. Lett. 107 (2011) 207402, doi:10.1103/PhysRevLett.107.207402.

[36] H. Przybylski, G. Borstel, Nonlocal density approximation to exchange and correlation in self-consistent bandstructure calculations: application to Cu, Solid State Commun. 49 (1984) 317–321, doi:10.1016/0038-1098(84)90577-5.

[37] H. Przybylski, G. Borstel, Nonlocal density approximation to exchange and correlation: ground state properties of solid copper and vanadium, Solid State Commun. 52 (1984) 713–716, doi:10.1016/0038-1098(84)90395-8.

[38] M. Alatalo, B. Barbiellini, M. Hakala, H. Kauppinen, T. Korhonen, M.J. Puska, K. Saarinen, P. Hautojärvi, R.M. Nieminen, Theoretical and experimental study of positron annihilation with core electrons in solids, Phys. Rev. B 54 (1996) 2397–2409, doi:10.1103/PhysRevB.54.2397.

[39] A. van Veen, H. Schut, J. de Vries, R.A. Hakvoort, M.R. Ijpma, Analysis of positron profiling data by means of "VEPFIT", in: AIP Conference Proceedings, Ontario (Canada), AIP, 1991, pp. 171–198, doi:10.1063/1.40182.

[40] A. van Veen, H. Schut, M. Clement, J.M.M. de Nijs, A. Kruseman, M.R. IJpma, VEPFIT applied to depth profiling problems, Appl. Surf. Sci. 85 (1995) 216–224, doi:10.1016/0169-4332(94)00334-3.

[41] M. Bertolaccini, L. Zappa, Source-supporting foil effect on the shape of positron time annihilation spectra, Nuov Cim. B 52 (1967) 487–494, doi:10.1007/BF02711092.

[42] P. Kirkegaard, M. Eldrup, Positronfit: a versatile program for analysing positron lifetime spectra, Danish Atomic Energy Commission Research Establishment, 1972 Risoe.

[43] P. Hautojärvi, C. Corbel, Positron spectroscopy of defects in metals and semiconductors, ENFI 125 (1995) 491–532, doi:10.3254/978-1-61499-211-0-491.

[44] P. Haas, F. Tran, P. Blaha, Calculation of the lattice constant of solids with semilocal functionals, Phys. Rev. B 79 (2009) 085104, doi:10.1103/PhysRevB.79.085104.

[45] G. Amarendra, R. Rajaraman, S. Rajagopalan, R. Suzuki, T. Ohdaira, Influence of defect-impurity complexes on slow positron yield of a tungsten moderator: positron annihilation, Auger, and SIMS study, Phys. Rev. B. 69 (2004) 094105, doi:10.1103/PhysRevB.69.094105.

[46] S. Zhu, Y. Xu, Z. Wang, Y. Zheng, D. Zhou, E. Du, D. Yuan, M. Fukuda, M. Mihara, K. Matsuta, T. Minamisono, Positron annihilation lifetime spectroscopy on heavy ion irradiated stainless steels and tungsten, J. Nucl. Mater. 343 (2005) 330–332, doi:10.1016/j.jnucmat.2004.11.024.

[47] J. Heikinheimo, K. Mizohata, J. Räisänen, T. Ahlgren, P. Jalkanen, A. Lahtinen, N. Catarino, E. Alves, F. Tuomisto, Direct observation of mono-vacancy and self-interstitial recovery in tungsten, APL Mater. 7 (2019) 021103, doi:10.1063/1.5082150.

[48] P.E. Lhuillier, M.F. Barthe, P. Desgardin, W. Egger, P. Sperr, Positron annihilation studies on the nature and thermal behaviour of irradiation induced defects in tungsten, Phys. Status Solidi (c) 6 (2009) 2329–2332, doi:10.1002/pssc.200982114.

[49] Y. Xu, Z. Wang, J. Zhu, T. Minamisono, K. Matsuta, Y. Zheng, D. Zhou, G. Xu, E. Du, Y. Fu, M. Fukuda, M. Mihara, S. Zhu, Radiation effects in stainless steel and tungsten for use in the ads spallation neutron source system, Mod. Phys. Lett. B 17 (2003) 147–151, doi:10.1142/S0217984903004981.

[50] M.J. Puska, R.M. Nieminen, Defect spectroscopy with positrons: a general calculational method, J. Phys. F Met. Phys. 13 (1983) 333–346, doi:10.1088/0305-4608/13/2/009.

[51] R.J. Wilson, A.P. Mills, Positron and positronium emission from tungsten (111), Phys. Rev. B 27 (1983) 3949–3954, doi:10.1103/PhysRevB.27.3949.

[52] M. Sidibe, Etude Du Comportement Du Tungstène Sous irradiation : Applications Aux Réacteurs De fusion, Phdthesis, Université d'Orléans, 2014 https://tel.archives-ouvertes.fr/tel-01068634 accessed January 7, 2021.

[53] J. Dryzek, D. Singleton, Implantation profile and linear absorption coefficients for positrons injected in solids from radioactive sources 22Na and 68Ge\68Ga„ Nucl. Instrum. Methods Phys. Res. Sect. B 252 (2006) 197–204, doi:10.1016/j.nimb.2006.08.017.

[54] Q. Xu, T. Yoshiie, H.C. Huang, Molecular dynamics simulation of vacancy diffusion in tungsten induced by irradiation, Nucl. Instrum. Methods Phys. Res. Sect. B 206 (2003) 123–126, doi:10.1016/S0168-583X(03)00697-9.

[55] K. Sato, R. Tamiya, Q. Xu, H. Tsuchida, T. Yoshiie, Detection of deuterium trapping sites in tungsten by thermal desorption spectroscopy and positron annihilation spectroscopy, Nuclear Mater. Energy 9 (2016) 554–559, doi:10.1016/j.nme.2016.09.014.

[56] P.-.E. Lhuillier, Etude Du Comportement De L'hélium Et Des Défauts Lacunaires Dans Le tungstène, Phdthesis, Université d'Orléans, 2010 https://tel.archives-ouvertes.fr/tel-00587482 accessed January 7, 2021.

[57] K. Sato, A. Hirosako, K. Ishibashi, Y. Miura, Q. Xu, M. Onoue, Y. Fukutoku, T. Onitsuka, M. Hatakeyama, S. Sunada, T. Yoshiie, Quantitative evaluation of hydrogen atoms trapped at single vacancies in tungsten using positron annihilation lifetime measurements: experiments and theoretical calculations, J. Nucl. Mater. 496 (2017) 9–17, doi:10.1016/j.jnucmat.2017.09.002.

[58] P.M.G. Nambissan, P. Sen, Positron annihilation study of the annealing behaviour of alpha induced defects in tungsten, Radiat. Eff. Defects Solids 124 (1992) 215–221, doi:10.1080/10420159208220193.

[59] O.V. Ogorodnikova, L.Y. Dubov, S.V. Stepanov, D. Terentyev, Yu.V. Funtikov, Yu.V. Shtotsky, V.S. Stolbunov, V. Efimov, K. Gutorov, Annealing of radiation-induced defects in tungsten: positron annihilation spectroscopy study, J. Nucl. Mater. 517 (2019) 148–151, doi:10.1016/j.jnucmat.2019.02.010.

[60] R.E. Stoller, M.B. Toloczko, G.S. Was, A.G. Certain, S. Dwaraknath, F.A. Garner, On the use of SRIM for computing radiation damage exposure, Nucl. Instrum. Methods Phys. Res. Sect. B 310 (2013) 75–80, doi:10.1016/j.nimb.2013.05.008.

[61] D.R. Mason, X. Yi, M.A. Kirk, S.L. Dudarev, Elastic trapping of dislocation loops in cascades in ion-irradiated tungsten foils, J. Phys.: Condens. Matter. 26 (2014) 375701, doi:10.1088/0953-8984/26/37/375701.

[62] F. Ferroni, X. Yi, K. Arakawa, S.P. Fitzgerald, P.D. Edmondson, S.G. Roberts, High temperature annealing of ion irradiated tungsten, Acta Mater. 90 (2015) 380–393, doi:10.1016/j.actamat.2015.01.067.